

Introduction

The Mars Science Laboratory (MSL) was protected during its Mars atmospheric entry by an instrumented heatshield that used NASA's Phenolic Impregnated Carbon Ablator (PICA) [1]. PICA is a lightweight carbon fiber/polymeric resin material that offers excellent performances for protecting probes during planetary entry. The Mars Entry Descent and Landing Instrument (MEDLI) suite on MSL offers unique in-flight validation data for models of atmospheric entry and material response. MEDLI recorded, among others, time-resolved in-depth temperature data of PICA using thermocouple sensors assembled in the MEDLI Integrated Sensor Plugs (MISP). These measurements have been widely used in the literature as a validation benchmark for state-of-the-art ablation codes [2,3,4]. The objective of this work is to perform an inverse estimate of the MSL heatshield material properties and aerothermal environment during Mars entry from the MISP flight data.

Porous material Analysis Toolbox based on OpenFOAM (PATO)

The computational model is a generic mass and heat transfer model for porous reactive materials containing several solid phases and a single gas phase. The detailed chemical interactions occurring between the solid phases and the gas phase are modeled at the pore scale assuming Local Thermal Equilibrium (LTE). This model is implemented in the Porous material Analysis Toolbox based on OpenFOAM (PATO) [5,6,7], a C++ top level module of the open source computational fluid dynamics software program **OpenFOAM**. The open source third party library **Mutation++**, produced by the von Karman Institute for Fluid Dynamics, is dynamically linked to compute equilibrium chemistry compositions and thermodynamic and transport properties [8]. For this study, the Theoretical Ablative Composite for Open Testing (TACOT) database developed by the TPS community was used to define the porous material properties. TACOT is a fictitious material that was inspired from low density carbon/phenolic ablators.

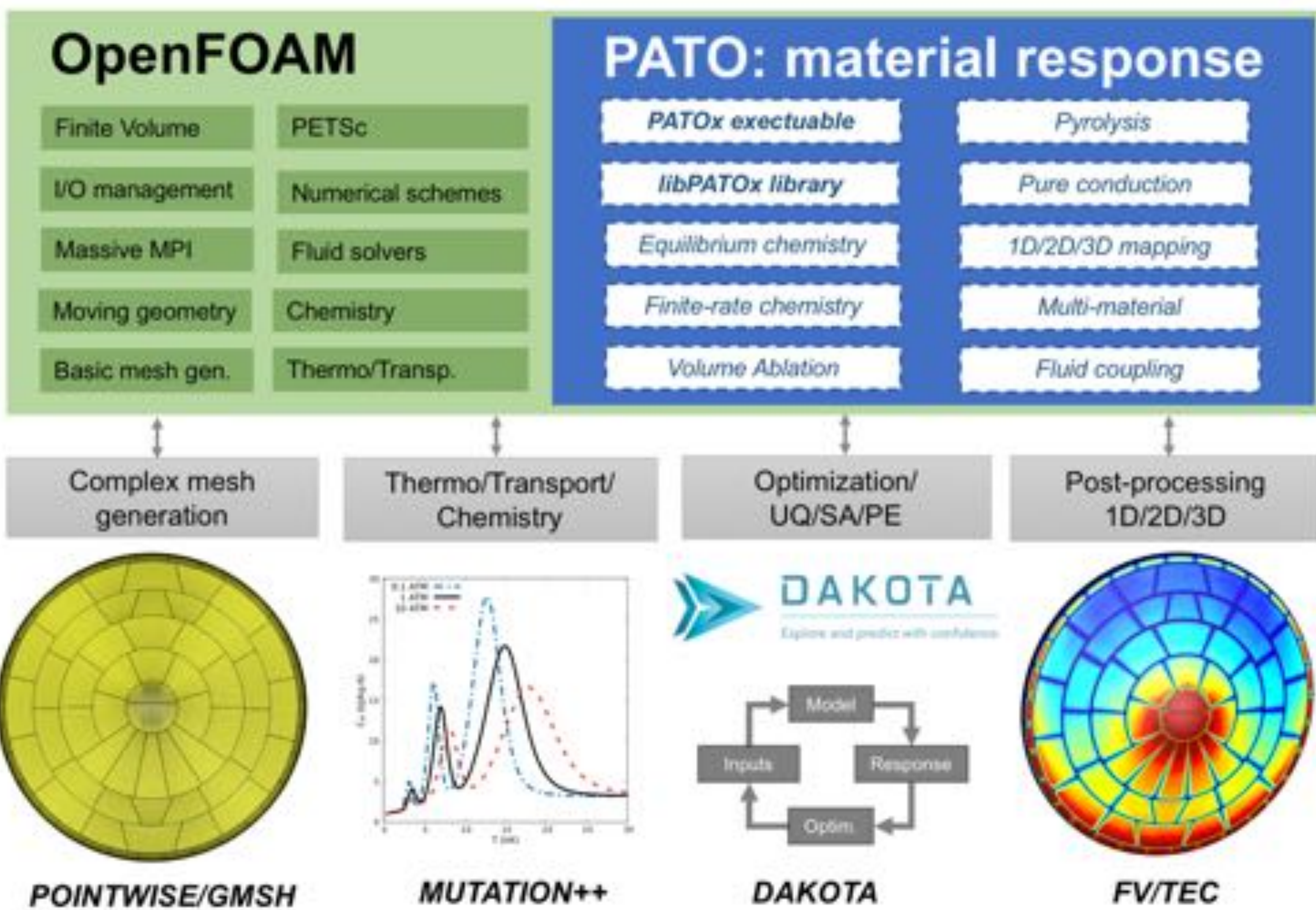


Fig. 1 Software architecture of the Porous material Analysis Toolbox based on OpenFOAM (PATO) version 3

TC1 driver results

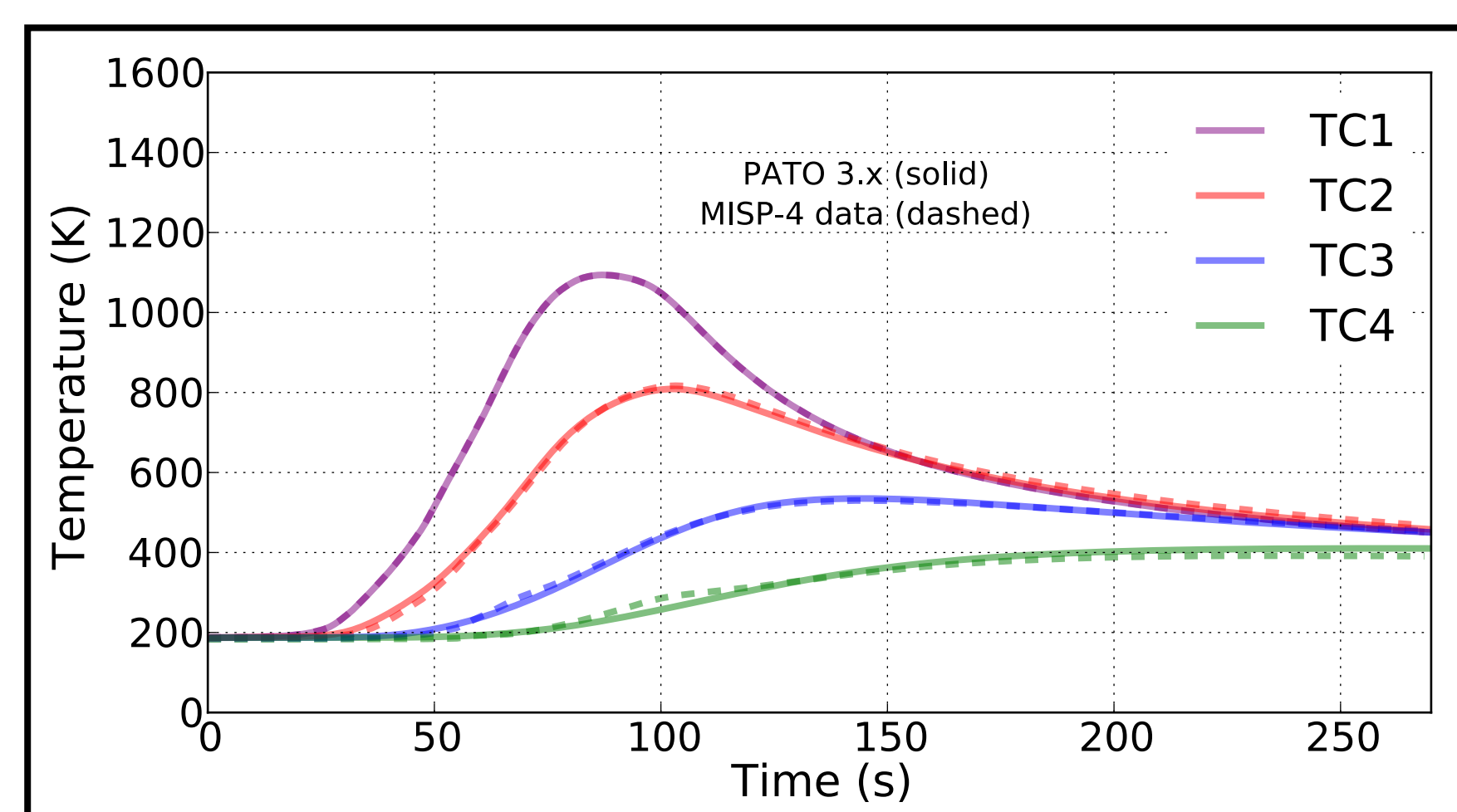


Fig. 6 Thermal response at MISP4 using TC1 driver

- Estimation of material properties
- Shallowest MISP 4 thermocouple
- Imposed wall temperature
- Equilibrium chemistry [7]
- Calibrated pyrolysis [9]
- TC4 hump due to water [10]

Inverse environment results

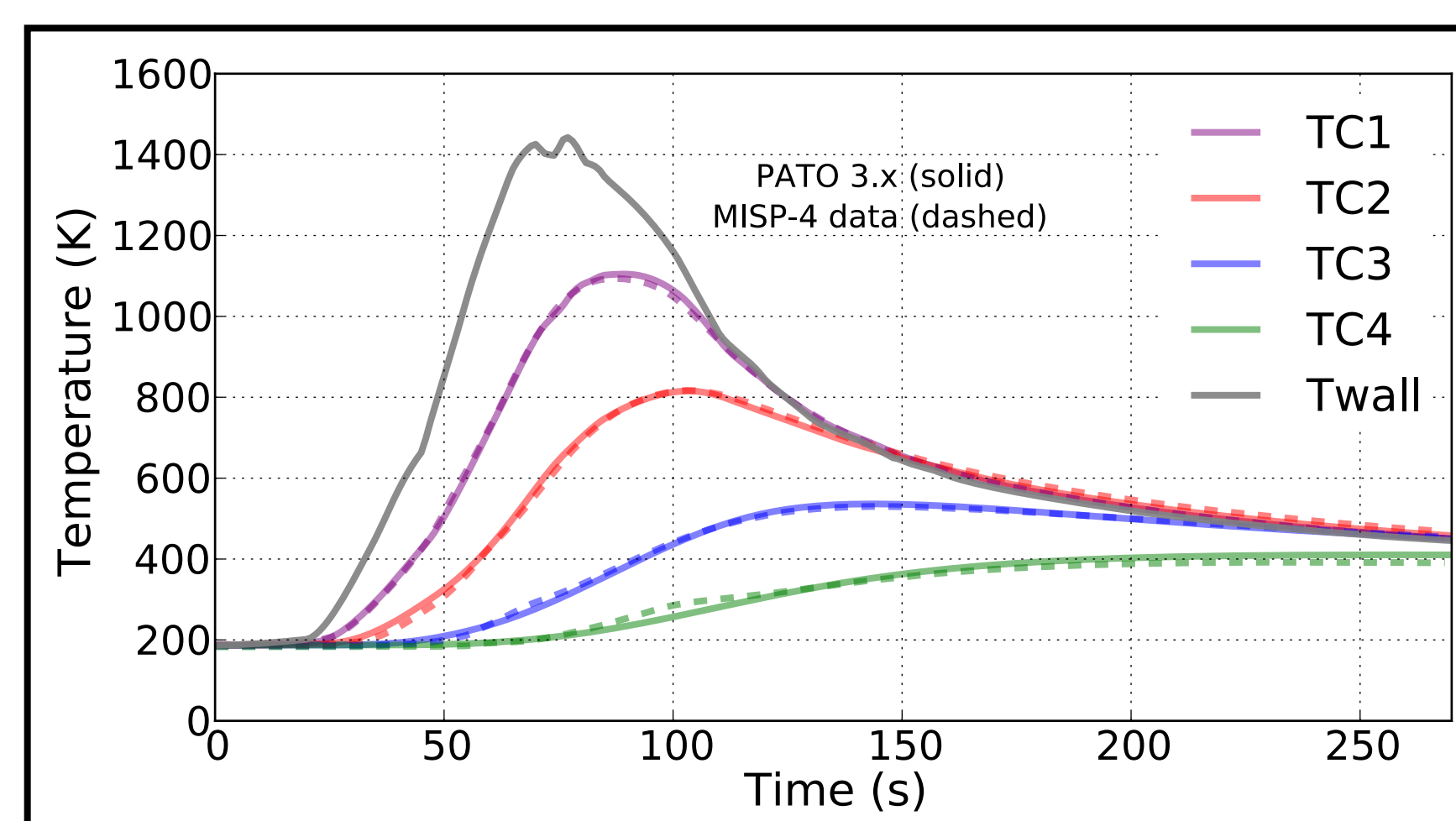


Fig. 7 Thermal response at MISP4 using the inverse environment

- Estimation of surface convective heat flux and char ablation rate
- Calculated temperature and recession using surface mass and energy balance
- Material properties from TC1 driver
- Note oscillations of wall temperature

Comparison to DPLR results

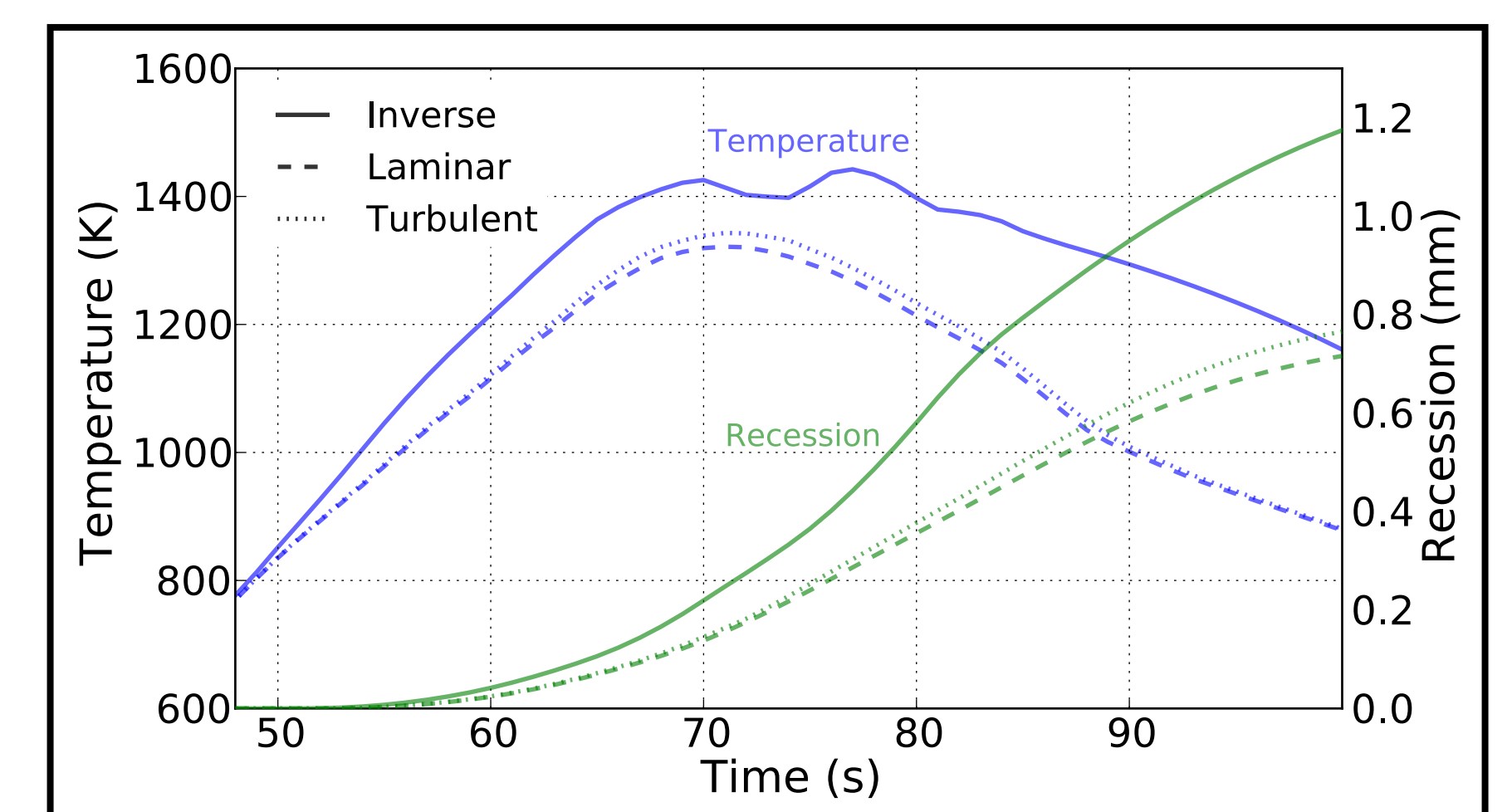


Fig. 8 Inverse and DPLR environment results

- Comparison of inverse derived environment with laminar and turbulent DPLR derived aerothermal environments
- DPLR environment underestimate temperature and recession at stag. point

Inverse estimation methodology

The inverse problem is handled by the **DAKOTA** library [12]. A multi-objective genetic algorithm and a trust-region method for nonlinear least squares are used to estimate key uncertain material parameters that influence the material response model. We follow the strategy of Mahzari et al [2,3] by using first the thermocouple driver approach to estimate uncertain parameters of the material model (**TC1 driver**). In this case, the temperature is imposed at the location of the shallowest MISP thermocouple. Then, the **aerothermal environment** is estimated by fitting the in-depth measured thermocouple response flight measurements. Finally, the laminar and turbulent environments from the Data Parallel Line Relaxation Code (DPLR) [11] are compared to the inverse solutions. This work represents an important milestone toward the development of validated **predictive capabilities** for designing Thermal Protection Systems for planetary probes.

NASA Release

DPLR: <https://software.nasa.gov/software/ARC-16021-1A>
PATO: <https://software.nasa.gov/software/ARC-16680-1>

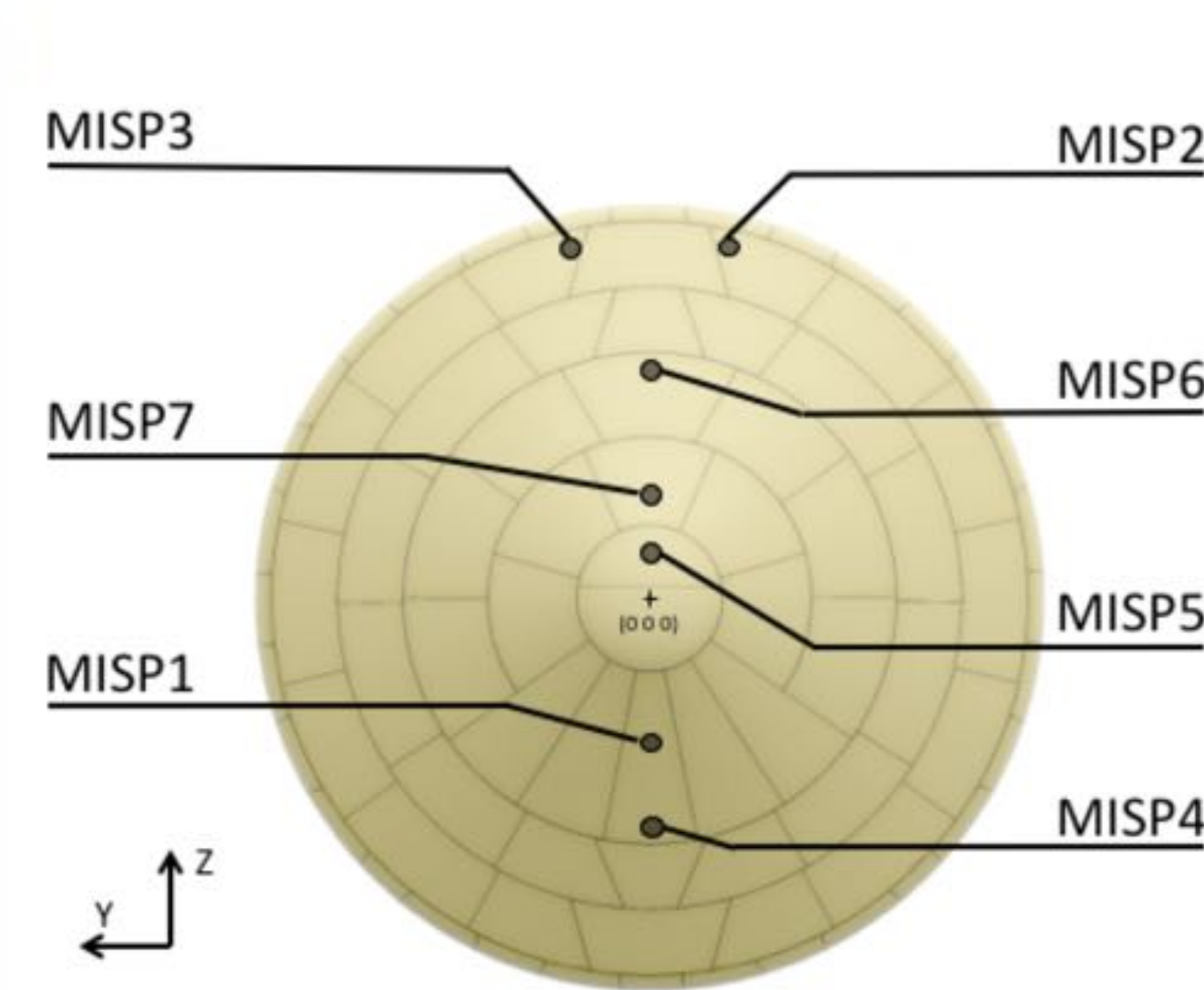


Fig. 2 MEDLI Integrated Sensor Plug (MISP) [7]



Fig. 3 MEADS pressure sensor [13]

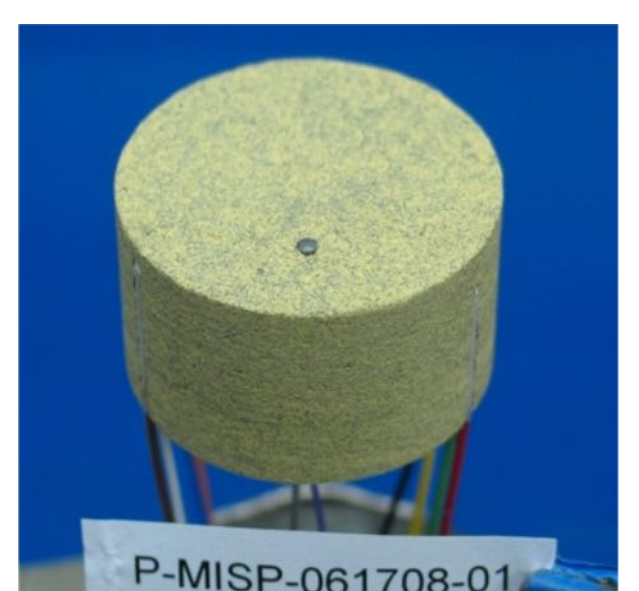


Fig. 4 MISP [13]

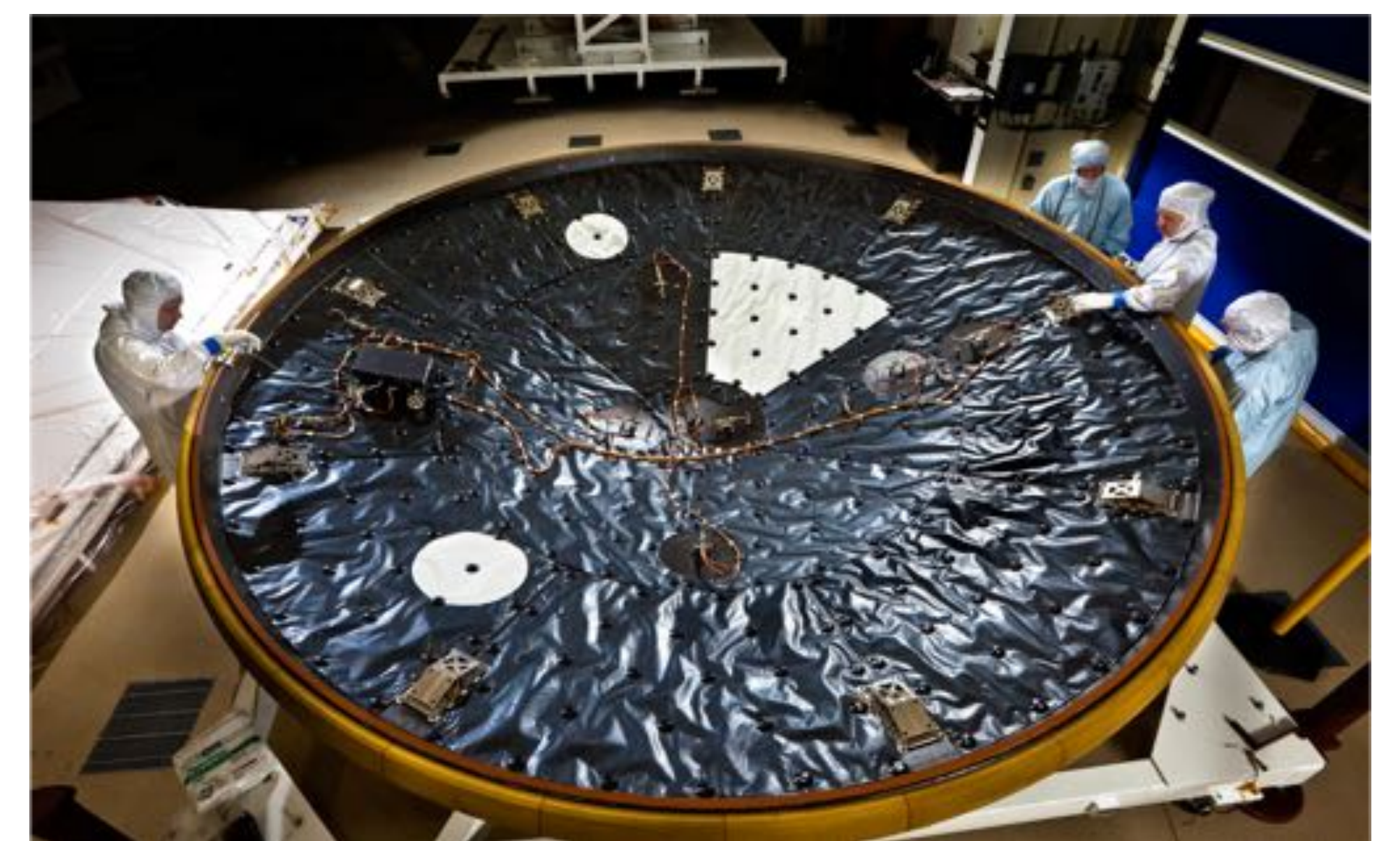


Fig. 5 MSL EDL Instrument (MEDLI) Suite assembling [13]

References

- [1] M.J. Wright et al. (2009), *AIAA Paper*, 2009-423.
- [2] M. Mahzari et al. (2013), *PhD Diss.*, Georgia Institute of Technology.
- [3] M. Mahzari et al. (2015), *Journal of Spacecraft and Rockets*, 52.4, 1203-1216.
- [4] T.R. White et al. (2013), *AIAA Paper*, 2013-2779.
- [5] J. Lachaud and N. N. Mansour (2014), *J Thermophys Heat Tran*, 28, 191-202.
- [6] J. Lachaud et al. (2017), *Int J Heat Mass Tran*, 108, 1406-1417.
- [7] J. B.E. Meurisse et al. (2018), *Aerosp Sci Technol*, 76, 497-511.
- [8] J. B. Scoggins and T. E. Magin (2014), *AIAA Paper*, 2014-2966.
- [9] F. Torres (2017), *Ablation Workshop*.
- [10] A.D. Omidy et al. (2016), *Journal of Thermophysics and Heat Transfer*, 473-478.
- [11] M.J. Wright et al. (2009), *DPLR Code User Manual*.
- [12] SANDIA (2014), <https://dakota.sandia.gov/documentation.html>, 05/15/18.
- [13] NASA, <https://mars.nasa.gov/msl/mission/instruments/atmosensors/medli>, 05/15/18.